Detection of terrestrial gamma ray flashes up to 40 MeV by the AGILE satellite

M. Marisaldi,[1] F. Fuschino,[1] C. Labanti,[1] M. Galli,[2] F. Longo,[3] E. Del Monte,[4]
G. Barbiellini,[3,5] M. Tavani,[4,6] A. Giuliani,[7] E. Moretti,[3] S. Vercellone,[8] E. Costa,[4]
S. Cutini,[9] I. Donnarumma,[4] Y. Evangelista,[4] M. Feroci,[4] I. Lapshov,[4,10] F. Lazzarotto,[4]
P. Lipari,[11,12] S. Mereghetti,[7] L. Pacciani,[4] M. Rapisarda,[13] P. Soffitta,[4] M. Trifoglio,[1]
A. Argan,[14] F. Boffelli,[15] A. Bulgarelli,[1] P. Caraveo,[7] P. W. Cattaneo,[15] A. Chen,[7]
V. Cocco,[4] F. D'Ammando,[4,6] G. De Paris,[14] G. Di Cocco,[1] G. Di Persio,[4] A. Ferrari,[16,17]
M. Fiorini,[7] T. Froysland,[6,16] F. Gianotti,[1] A. Morselli,[18] A. Pellizzoni,[19] F. Perotti,[7]
P. Picozza,[18] G. Piano,[4,6,18] M. Pilia,[20] M. Prest,[20,21] G. Pucella,[4] A. Rappoldi,[15]
A. Rubini,[4] S. Sabatini,[18] E. Striani,[4,6,18] A. Trois,[4] E. Vallazza,[5] V. Vittorini,[4]
A. Zambra,[7,16] D. Zanello,[11] L. A. Antonelli,[9] S. Colafrancesco,[9] D. Gasparrini,[9]
P. Giommi,[9] C. Pittori,[9] B. Preger,[9] P. Santolamazza,[9] F. Verrecchia,[9] and L. Salotti[22]

[1]   We report the detection by the Astrorivelatore Gamma a Immagini Leggero (AGILE) satellite of terrestrial gamma ray flashes (TGFs) obtained with the minicalorimeter (MCAL) detector operating in the energy range 0.3–100 MeV. We select events typically lasting a few milliseconds with spectral and directional selections consistent with the TGF characteristics previously reported by other space missions. During the period 1 June 2008 to 31 March 2009 we detect 34 high-confidence events showing millisecond durations and a geographical distribution peaked over continental Africa and Southeast Asia. For the first time, AGILE-MCAL detects photons associated with TGF events up to 40 MeV. We determine the cumulative spectral properties of the spectrum in the range 0.5–40 MeV, which can be effectively described by a Bremsstrahlung spectrum. We find that both the TGF cumulative spectral properties and their geographical distribution are in good agreement with the Reuven Ramaty High Energy Solar Spectroscopic Imager (RHESSI) results.

1. Introduction

[2]   Terrestrial gamma ray flashes (TGFs) are one of the most intriguing phenomena in the geophysical sciences. Although their origin is terrestrial, they were discovered and, to this day, have only been observed by satellites dedicated to high-energy astrophysics. *Fishman et al.* [1994] reported the discovery of TGFs by the Burst And Transient Source Experiment (BATSE), sensitive above 20 keV [*Fishman et al.*, 1989], on board the NASA Compton Gamma-Ray Observatory (CGRO). These events are described as millisecond time scale bursts of gamma rays with the incoming direction compatible with the Earth and a spectral hardness typically much higher than that of cosmic gamma ray bursts.

[1]IASF, INAF, Bologna, Italy.
[2]ENEA, Bologna, Italy.
[3]Dipartimento di Fisica, Università di Trieste, Trieste, Italy.
[4]IASF, INAF, Rome, Italy.
[5]INFN, Trieste, Italy.
[6]Dipartimento di Fisica, Università degli Studi di Roma "Tor Vergata," Rome, Italy.
[7]IASF, INAF, Milan, Italy.
[8]IASF, INAF, Palermo, Italy.
[9]ASI Science Data Center, Frascati, Italy.
[10]IKI, Moscow, Russia.
[11]INFN, Rome, Italy.
[12]Dipartimento di Fisica, Università degli Studi di Roma "La Sapienza," Rome, Italy.
[13]ENEA, Frascati, Italy.
[14]INAF, Rome, Italy.
[15]INFN, Pavia, Italy.
[16]CIFS, Turin, Italy.
[17]Dipartimento di Fisica, Università Torino, Turin, Italy.
[18]INFN, Rome, Italy.
[19]Osservatorio Astronomico di Cagliari, INAF, Capoterra, Italy.
[20]Dipartimento di Fisica, Università dell'Insubria, Como, Italy.
[21]INFN, Milan, Italy.
[22]Agenzia Spaziale Italiana, Rome, Italy.

Inan et al. [1996] and *Cohen et al.* [2006] showed the direct association of TGFs with lightning and thunderstorm activity by means of timing and spatial correlation of some of the BATSE TGFs with lightning strokes localized by their signature at VLF frequencies (sferics). Due to limitations in its trigger logic architecture, BATSE was able to detect only 76 TGFs in 9 years of operations. TGFs were then observed at energies up to 20 MeV by the spectrometer on board the Reuven Ramaty High Energy Solar Spectroscopic Imager (RHESSI), as reported in the work by *Smith et al.* [2005]. Although each RHESSI event includes many fewer photons than the BATSE TGFs, because of the significant differences in the effective area between the two instruments, RHESSI produced a breakthrough in the TGF sample statistics detecting 820 TGFs from 2002 through 2008, as reported by *Grefenstette et al.* [2009] in the first RHESSI TGF catalog. This increase in the TGF detection rate is mainly due to the fact that all RHESSI data are downloaded on a photon-by-photon basis without the need for any onboard trigger, whereas BATSE required at least a trigger on the minimum sampling time window of 64 ms, much larger than the average TGF duration, therefore selecting only bright high-significance TGFs.

[3] More than 15 years after their discovery, the source mechanism and production sites of TGFs are still under debate. After the first BATSE observations, it was suggested that TGFs could be related to discharges at high altitudes possibly associated with sprites [*Roussel-Dupré and Gurevich*, 1996; *Nemiroff et al.*, 1997], but *Dwyer and Smith* [2005] showed that the observed RHESSI TGF cumulative spectrum is compatible with gamma rays produced much deeper in the atmosphere at 15–21 km altitude above sea level. *Dwyer and Smith* [2005] also showed that the spectrum is consistent with bremsstrahlung emission from a population of high-energy electrons produced by means of relativistic runaway electron avalanche (RREA) multiplication [*Gurevich et al.*, 1992]. This fine spectral modeling has been possible because of the RHESSI higher spectral resolution than BATSE for time-tagged events. Moreover, *Cummer et al.* [2005] showed that the charge moment change connected to lightning strokes associated with TGFs, as implied by sferics observations, is too low to be responsible for sprite production, confirming that the correlation between sprites and TGFs is not straightforward, if it exists. Recently, *Dwyer* [2008] put further constraints on the production mechanism of TGFs suggesting that either relativistic feedback or runaway electron production in high electric fields may play a role, and excluding a major contribution from extensive air showers of cosmic rays in the initiation process. Concerning the emission geometry, analysis of both BATSE and RHESSI data suggest that the initial gamma ray emission is beamed [*Østgaard et al.*, 2008; *Hazelton et al.*, 2009], although the degree of beaming is not yet clearly assessed.

[4] *Grefenstette et al.* [2008, 2009] showed that both BATSE and RHESSI data are affected by instrumental effects such as dead time and pileup, because of the extremely high TGF fluxes. In light of these effects, all previous results concerning timing and spectral characteristics of TGFs need to be revised, as recently pointed out by *Østgaard* [2009].

[5] Recently, the AGILE and Fermi satellites, both devoted to gamma ray astrophysics, have reported the detection of

TGFs from space. AGILE reported the detection of short bursts of gamma rays with characteristics compatible with those of TGFs shortly after the activation of the onboard trigger logic in November 2007 [*Fuschino et al.*, 2009], and later after the extension of the trigger logic to very short time scales [*Longo et al.*, 2008; *Marisaldi et al.*, 2009]. The Fermi team reported the detection of TGFs with the GBM instrument [*Fishman and Smith*, 2008; *Fishman*, 2009]. In this paper we present the results of the first nine months of observation of TGFs with AGILE after the extension of the trigger logic to very short time scales. In the following we will describe the AGILE payload (section 2) and the trigger algorithm and the selection criteria applied for TGF detection (section 3). Then, the properties of the AGILE TGFs sample will be described (section 4) and a comparison with the results already published by RHESSI will be discussed (section 5).

2. AGILE Payload

[6] Astrorivelatore Gamma a Immagini Leggero (AGILE) (AGILE mission Web page: http://agile.rm.iasf.cnr.it/) is a space mission of the Italian Space Agency (ASI) devoted to astrophysics in the gamma ray energy range 30 MeV to 30 GeV, with a monitor in the X-ray band 18–60 keV. *Tavani et al.* [2008, 2009] report a description of the AGILE mission and its main scientific objectives. AGILE was launched on 23 April 2007 in a low-Earth orbit at 550 km altitude with 2.5° inclination.

[7] The AGILE payload is composed of the following detectors: (1) a tungsten-silicon tracker (ST) [*Prest et al.*, 2003], with a large field of view, good time resolution, sensitivity and angular resolution; (2) a silicon based X-ray detector, SuperAGILE (SA) [*Feroci et al.*, 2007], for imaging in the range 18–60 keV; (3) a CsI(Tl) minicalorimeter (MCAL) [*Labanti et al.*, 2009] for the detection of gamma rays in the range 300 keV to 100 MeV; and (4) an anticoincidence (AC) system [*Perotti et al.*, 2006] made with plastic scintillator layers for the rejection of charged particle events. The scientific payload is completed by the Payload Data Handling Unit (PDHU) [*Argan et al.*, 2004] that takes care of data acquisition of the various detectors. ST and MCAL form the so-called Gamma-Ray Imaging Detector (GRID) for observations in the energy range 30 MeV to 30 GeV.

[8] All the TGFs reported in this paper were detected by the MCAL instrument. MCAL is composed of 30 CsI(Tl) scintillator bars (dimensions: $15 \times 23 \times 375$ mm^3 each) read out by two custom PIN Photodiodes (PD) coupled one at each small side. The bars are arranged in two orthogonal layers, for a total thickness of 1.5 radiation lengths. Although MCAL can work in conjunction with the ST (GRID operative mode) it is also equipped with a self-triggering operative mode and onboard trigger logic making it an all-sky transient monitor in the 300 keV to 100 MeV energy range (BURST operative mode). Both operative modes are active at the same time. The trigger logic [*Fuschino et al.*, 2008] is active on several time scales spanning 4 orders of magnitude from 8 s down to 293 μs, allowing the detection of a wide variety of transient phenomena from long cosmic gamma ray bursts (GRBs) to TGFs at the submillisecond time scale. When a trigger is issued, MCAL data are sent to telemetry on a photon-by-photon basis for a time window of 60 s centered at the trigger
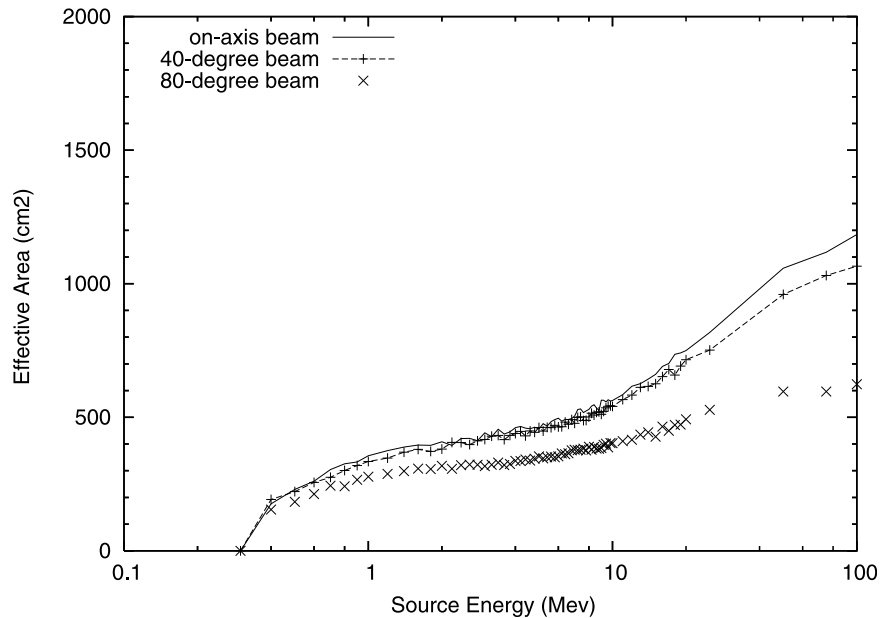
Figure 1. Minicalorimeter (MCAL) total effective area as a function of energy [from *Labanti et al.*, 2009].

time including, for every photon, energy information and a time tag with 1 μs accuracy; in this way, timing and energy binning is limited by counting statistics only. Figure 1 reports the total MCAL effective area as a function of the incident photon energy, computed by means of Monte Carlo simulations for parallel photon beams at different incidence angles, as reported in work by *Labanti et al.* [2009]. Both full energy absorption and partial energy loss of photons have been considered for the effective area calculation. This plot refers to MCAL operated as a self-triggering detector, i.e., in the so-called BURST mode, which is the operative mode considered throughout this work. The effective area remains almost constant up to about 70° off-axis. The effective area estimates have been verified using GRBs detected by different spacecrafts (M. Marisaldi et al., manuscript in preparation, 2010). *Marisaldi et al.* [2008a, 2008b] report the MCAL in-flight performance and its GRB detection capabilities after more than one year of operation in space.

[9] Since the activation of the trigger logic on 64 ms and longer time windows (December 2007 and then steadily active since 5 February 2008), several events have been detected exhibiting timing characteristics compatible with those of TGFs. These preliminary detections have been reported by *Fuschino et al.* [2009] and will be discussed later in the context of the new results. Since June 2008, the onboard trigger logic has also been enabled on the very short time scales of 16 ms, 1 ms and 293 μs, thus opening an observational window for fainter short time scale transient events.

[10] The onboard time-tagging accuracy for the AGILE photons is ~1 μs. The effective absolute time resolution has proven to be better than ~200 μs, after accurate timing observations of the Vela pulsar, as described in detail by *Pellizzoni et al.* [2009]. At present, there are no known issues that prevent the achievement of an absolute time resolution

as good as ~50 μs, provided that adequate counting statistics are obtained.

3. Trigger Algorithm and Selection Criteria

[11] The trigger logic on time scales of 16 ms and 293 μs was enabled and configured in mid June 2008. The trigger logic for the 1 ms time scale was properly configured on 2 March 2009, and since then the trigger logic on all time scales has been active and working properly. After a threshold scan to verify the trigger rate compliance with the telemetry budget, the following thresholds were set in the onboard trigger logic configuration: 22 counts for the 16 ms, 10 counts for the 1 ms and 8 counts for the 293 μs time scales. The average background rate is ~350 counts/s with a smooth 10% modulation along the orbit except in the South Atlantic Anomaly (SAA), where the trigger logic is disabled.

[12] During the period between 18 June 2008 and 31 March 2009, MCAL triggered several thousand events on the 16 ms time scale or shorter, with an average rate of 6.8 triggers/orbit, i.e., ~95 triggers/day. The trigger threshold has been deliberately kept as low as possible, but still fully compliant with the telemetry budget. Note that this is the first time that trigger logic on time scales shorter than 16 ms has been implemented on a space mission. Consequently, in order not to miss any faint events by using an excessively conservative onboard threshold, we decided to leave event selection to the on-ground analysis. In fact, a large fraction of the triggers are due to either statistical fluctuations or electronic noise, and a careful selection strategy has to be applied. It was soon discovered that a class of triggers is strictly related to a particular payload status clearly marked in-housekeeping data, and could be easily rejected. Moreover, due to an initial issue with the onboard software for the 1 ms time window, some data are missing for those events triggering on this time
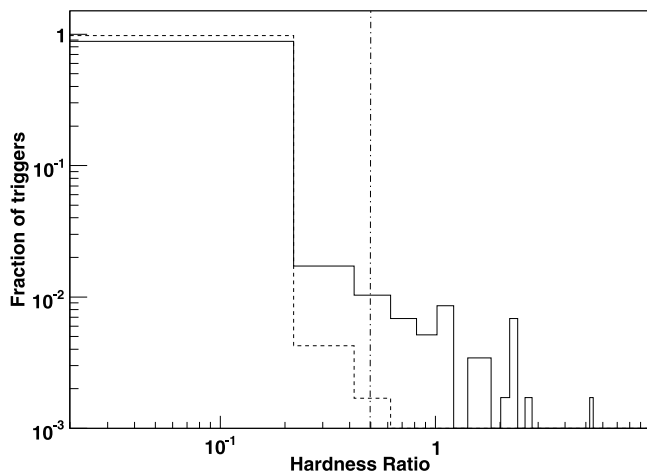
Figure 2. Normalized hardness ratio distribution for triggers of instrumental origin (dashed line) and for the other triggers (solid line). Only events with at least 10 counts have been selected. The vertical dot-dashed line marks the HR = 0.5 value.

scale, so these events were not considered for the period before the software update on 2 March 2009. Since this issue affects also the events bright enough to trigger both the 16 ms and 1 ms time scales, the selected population is possibly biased toward longer, less bright events.

[13] Further criteria for candidate selection are based on hardness ratio and fluence. The hardness ratio HR is defined as follows:

$$HR = \frac{\text{number of counts with } E \geq 1.4 \text{ MeV}}{\text{number of counts with } E < 1.4 \text{ MeV}}$$

We decided to use HR instead of average energy as a rough estimator of the spectral hardness because a single high-energy photon can significantly influence the average energy, given the large MCAL dynamic range. Moreover, a cut on HR is necessary for the rejection of triggers of instrumental origin, to avoid contamination of the sample with spurious triggers. In fact, the procedure for instrumental trigger identification is not 100% efficient, because of the limited timing accuracy of housekeeping data. For instrumental triggers on the 16 ms time scale the average HR is 0.07 and only one event out of 397 exhibits HR > 0.2. HR $\simeq$ 0.5 for the MCAL background, quite stable along the orbit except for the passage through the SAA. We have chosen to select events with HR $\geq$ 0.5, as well as requiring at least 10 photons in the burst duration as a cut on the overall number of counts. Figure 2 shows the normalized hardness ratio distribution for triggers of instrumental origin and for the other triggers, for events with at least 10 counts. The vertical line evidences the HR cut used in this work. The HR cut chosen is quite severe, but it is expected to minimize the contribution of spurious instrumental triggers. All events satisfying these selection criteria were visually inspected to exclude further contamination from instrumental effects, as well as to provide a human double-check of the start time and duration assigned

to each event by the automatic analysis procedure. Since the photons of a TGF candidate are typically very well clustered in time while the background ($\simeq$0.35 counts/ms) contributes with sparse, randomly displaced counts, an automatic procedure searches for the bin with the maximum number of counts around the trigger time (typical time bin 200 μs; 500 μs for weak candidates) and then finds the region of connected bins around the maximum. The burst duration is basically defined as the duration of this cluster of connected bins. The only exception to this algorithm is allowed if a photon with energy greater than 1.4 MeV is found after a single bin with zero counts; in this case the corresponding bin is included in the burst and the event duration is extended accordingly. According to the selection criteria described above a total number of 34 events have been selected over the considered period, i.e., about 4 events/month.

4. AGILE-MCAL Detections

4.1. Trigger Properties

[14] Tables 1, 2 and 3 report the main characteristics of the selected events. Every event is uniquely identified by a trigger ID composed of two integers separated by a dash. The first number indicates the AGILE orbit and the second one is the trigger index within that orbit. For each event, Table 1 reports the trigger time, the geographical coordinates of the AGILE footprint, the local time, the angle between the AGILE pointing direction and the nadir, as well as the fired trigger configuration. Table 2 reports the main physical properties of each event, while Table 3 summarizes the average characteristics of the 34 selected events. It must be noted that all the triggers obtained on longer time windows (64 ms) and previously presented [*Fuschino et al.*, 2009] do not meet the HR selection criteria developed for the sample of triggers at shorter time scale. Some of them can be explained as due to electronic noise, according to the improved analysis later developed for the short time scale triggers. Nonetheless the four brightest events reported in the previous paper are expected to be real but, since they are significantly softer, brighter and longer than the current sample, we believe that they can be originated by different physical phenomena. For this work we thus consider only triggers on the 16 ms time scale and shorter, satisfying the selection criteria stated above.

[15] The fired trigger configuration consists of three binary flags, one for each of the three very short time windows tested by the trigger logic (293 μs, 1 ms and 16 ms). A value of 1 indicates that the trigger logic on the corresponding time window issued a valid trigger. Before March 2009 no events with the 1 ms trigger fired were selected, because of the different event acquisition configuration mentioned in section 3. Since the configuration update on 2 March 2009, five selected events out of nine present the 1 ms trigger fired. If this trend is confirmed in the next months of observation, this means that the TGF candidates detection rate has been more than doubled by this configuration improvement.

[16] The light curves integrated over the entire energy range of the detector for some of the most significant events are reported in Figure 3, together with the plot of energy versus time for all photons detected.

[17] Figure 4 shows the geographical distribution of the trigger sample. It must be pointed out that, due to the low inclination of the AGILE orbit, only a very narrow region

Table 1. Geographical and Trigger Properties of the Selected Candidates

Trigger	Date	Time (UT)	Longitude (deg)	Latitude (deg)	Local Time	θ[a] (deg)	0.293 ms	1 ms	16 ms
5945-3	17 Jun 2008	1520:14	26.25	0.88	17.09	53.7	0	0	1
6630-2	5 Aug 2008	0231:26	64.77	2.12	6.84	137.4	0	0	1
6896-6	23 Aug 2008	2345:14	115.44	−1.47	7.45	98.0	0	0	1
7249-4	18 Sep 2008	0025:21	6.75	−0.66	0.87	76.1	0	0	1
7330-5	23 Sep 2008	1812:52	21.67	−1.74	19.66	142.9	0	0	1
7467-3	3 Oct 2008	0954:56	119.96	0.49	17.91	151.0	1	0	1
7568-1	10 Oct 2008	1150:36	99.32	2.43	18.46	148.5	0	0	1
7617-4	14 Oct 2008	0134:16	250.84	2.34	18.29	46.4	0	0	1
7728-6	21 Oct 2008	2138:21	111.51	−0.98	5.07	11.7	1	0	1
7794-10	26 Oct 2008	1509:14	26.81	−0.64	16.94	166.4	1	0	1
7876-7	1 Nov 2008	1041:11	50.83	−0.91	14.08	125.6	0	0	1
7919-1	4 Nov 2008	1022:33	110.15	−2.41	17.72	140.7	0	0	1
7973-6	8 Nov 2008	0612:35	114.48	−2.40	13.84	59.5	0	0	1
8087-3	16 Nov 2008	0834:45	230.09	2.20	23.92	77.3	0	0	1
8204-5	24 Nov 2008	1612:15	17.93	2.47	17.40	146.9	1	0	1
8304-5	1 Dec 2008	1811:04	9.34	0.37	18.81	132.9	1	0	1
8385-2	7 Dec 2008	1049:17	140.77	−2.16	20.21	117.8	1	0	1
8594-7	22 Dec 2008	0718:49	24.91	−0.82	8.97	75.3	0	0	1
8742-16	1 Jan 2009	1855:26	21.51	2.43	20.36	113.3	1	0	1
8845-9	9 Jan 2009	0159:56	12.21	−2.42	2.81	48.2	0	0	1
8958-8	17 Jan 2009	0207:15	12.84	−1.25	2.98	120.7	1	0	1
9068-7	24 Jan 2009	2108:44	13.84	−1.50	22.07	77.5	0	0	1
9506-9	24 Feb 2009	2148:21	12.44	−2.04	22.64	83.4	0	0	1
9512-2	25 Feb 2009	0758:35	5.64	1.05	8.35	88.9	1	0	0
9574-10	1 Mar 2009	1724:29	10.84	−1.20	18.13	30.8	1	0	0
9588-10	2 Mar 2009	1714:14	16.59	−1.61	18.34	31.9	1	0	0
9669-1	8 Mar 2009	0941:27	110.13	−2.31	17.03	34.1	1	0	1
9672-2	8 Mar 2009	1446:02	105.31	−1.49	21.79	62.5	1	1	0
9765-2	15 Mar 2009	0602:24	351.09	1.76	5.45	148.7	1	0	1
9769-6	15 Mar 2009	1301:03	28.05	−2.44	14.89	55.0	1	1	1
9846-7	20 Mar 2009	2328:50	293.48	1.13	19.05	31.0	0	0	1
9848-8	21 Mar 2009	0313:27	6.65	0.92	3.67	134.3	1	1	1
9885-1	23 Mar 2009	1652:16	100.07	2.18	23.54	81.3	1	1	0
9902-10	24 Mar 2009	2157:14	138.61	−2.20	7.20	148.8	1	1	0

[a]Angle between the nadir and the AGILE pointing direction.

along the equator has been covered; no high-latitude coverage can be obtained. There is evidence for events clustering on the African continental region and the Southeast Asia. In particular, the events recorded over Africa (in the longitude interval 0–30°) and Southeast Asia (in the longitude interval 90–120°) account for about half and one third of the total recorded events, respectively. The lack of events over South America is due to the automatic disabling of the trigger logic as AGILE enters the SAA.

4.2. Cumulative Spectrum

[18] Figure 5 shows the cumulative spectrum obtained by summing all the counts in the TGF duration intervals reported in Table 2, for a net total exposure of about 51 ms, after background subtraction. The spectrum was rebinned in order to have at least 20 counts per bin, to allow us to use the χ^2 minimization fitting technique and ensure the validity of Gaussian statistics. The cumulative background was obtained summing the counts in a 20 s time interval starting from 1 s after the trigger time, for each TGF. This method was chosen because, for some of the candidates, not all of the data are available for the nominal time period before the trigger time. Considering the low (~0.35 counts/ms) and stable, at least on a time scale of minutes, background, this calculation method should not affect the results significantly. In fact, 97% of the total counts per unit time are represented by the source, i.e., the TGF photons.

[19] A flattening in the spectrum at low energy can be observed. Despite the relatively high (300 keV) MCAL energy threshold and the fact that energy resolution gets worse close to the threshold, thus smearing the photons at low energy, we do not exclude the possibility of providing information about the depth of TGF production sites using the MCAL energy spectrum below ~3 MeV, following the approach outlined in the work by *Dwyer and Smith* [2005].

[20] At energies above 10 MeV a spectral cutoff is evident. Since each MCAL bar has a dynamic range extended up to 100 MeV, and for multiple counts the total energy is obtained summing the energy deposited in all triggered bars, MCAL is in principle an optimal detector for characterizing the high-energy part of the TGF spectra. Of course, owing to the limited thickness of the detector (1.5 radiation lengths) most of the interactions for photons above 10 MeV will give rise only to partial absorption in MCAL, and the response matrix at these energy is strongly nondiagonal.

[21] A question may thus arise whether the observed cutoff is a real physical feature or may be ascribed to an improper computation of the response matrix, namely an overestimation of the effective area at high energy. In fact, this energy range cannot be easily tested in orbit using, for example, cosmic GRBs, which rarely give significant signal above 10 MeV in MCAL. However, a comprehensive on-ground calibration campaign of the GRID detector was performed at the Beam Test Facility of the INFN Laboratori Nazionali

Table 2. Physical Properties of the Selected Candidates

Trigger	Duration (ms)	Number of Counts	Peak Flux (Counts/ 200 μs)	Average Energy (MeV)	Hardness Ratio	Maximum Energy (MeV)
5945-3	1.8	21	4	2.8	1.1	16.7
6630-2	3.6	18	5	4.6	1.3	23.7
6896-6	2.6	13	3	4.6	0.6	33.0
7249-4	3.0	12	4	9.9	1.4	43.2
7330-5	2.6	18	3	2.6	0.8	9.8
7467-3	1.6	23	8	4.2	1.3	16.6
7568-1	2.4	17	6	2.1	0.9	5.8
7617-4	2.4	11	2	5.0	0.8	33.4
7728-6	0.4	10	7	5.4	2.3	12.5
7794-10	1.0	19	7	4.8	2.2	14.3
7876-7	1.8	11	5	4.5	0.8	26.2
7919-1	1.4	17	4	4.5	3.3	17.1
7973-6	1.2	16	4	3.5	1.7	10.2
8087-3	1.6	14	5	4.7	0.8	20.5
8204-5	1.0	19	8	4.1	1.7	14.7
8304-5	0.8	20	8	3.3	1.9	16.2
8385-2	1.0	18	9	2.6	0.8	11.9
8594-7	1.6	15	5	4.3	1.5	13.8
8742-16	1.0	17	8	4.4	1.8	13.9
8845-9	1.8	22	6	3.1	1.4	10.1
8958-8	2.0	33	7	4.0	1.8	25.1
9068-7	1.6	11	3	4.9	2.7	11.8
9506-9	1.2	18	5	4.5	2.6	14.4
9512-2	0.6	10	6	2.4	0.7	11.3
9574-10	0.8	13	5	4.0	1.2	10.1
9588-10	0.6	13	7	2.2	1.6	5.7
9669-1	2.6	23	7	3.5	1.3	12.8
9672-2	0.6	11	8	3.9	2.7	19.8
9765-2	0.6	19	10	2.9	0.7	16.1
9769-6	1.0	13	5	3.9	1.6	14.5
9846-7	2.0	23	6	4.0	1.9	20.1
9848-8	1.0	18	7	3.0	1.3	12.2
9885-1	0.8	14	8	3.5	1.8	12.3
9902-10	0.8	12	4	1.8	0.5	5.3

di Frascati, Italy, using high-energy photons obtained from thin target bremsstrahlung of nearly monoenergetic electrons of energy up to 600 MeV. Despite the fact that this test campaign was mainly aimed at the calibration of the AGILE silicon tracker, several runs were acquired with MCAL in self-triggering mode. The beam spectrum recorded by MCAL can be fit with a simple power law model between 10 and 80 MeV and no significant deviations induced by an incorrect response matrix are evident.

[22] A tentative fit of the count spectrum with a cutoff power law model ($F(E) \propto E^{-\alpha} e^{-E/\beta}$), reasonably representing a bremsstrahlung spectrum, was performed in the energy range 500 keV to 40 MeV. The best fit model yields a spectral index $\alpha = 0.39^{+0.27}_{-0.32}$ and a high-energy cutoff energy $\beta = 8.5^{+3.2}_{-2.2}$ MeV, with a reduced χ^2 of 1.4 with 18 degrees of freedom. All quoted errors are at the 90% confidence level. The fit was obtained using a response matrix obtained for a 40° off-axis angle with respect to the center of the AGILE field of view. Figure 5 (top) shows this best fit model convolved with the instrumental response together with the background-subtracted cumulative count spectrum, Figure 5 (bottom) showing the residuals distribution. The same fitting procedure was repeated for off-axis angles between 0 and 155°, yielding spectral parameters consistent with those reported above, as expected because of the moderate angular dependence of the MCAL response at high energy. Although

this model is purely empirical, it is useful for the comparison between the MCAL and RHESSI cumulative spectra, as discussed in section 5. A fit of the count spectrum with a simple power law in the 1–10 MeV energy range does not give acceptable results. Since the selected events exhibit a wide range of off-axis angles with respect to the AGILE pointing, the use of a response matrix for isotropic photons might yield more accurate results.

[23] A total number of 47 photons with energy higher than 10 MeV and 8 photons with energy higher than 20 MeV are detected in the selected TGF sample. The expected number of background counts for the same exposure time (51 ms) in the same energy ranges is 2.3 and 1.3, respectively. The maximum energy recorded is 43 MeV, for a photon detected in trigger 7249-4. This trigger, whose light curve is shown in Figure 3g, despite being characterized by a relatively low number of total detected counts, exhibits a large fraction of photons above 1 MeV and fully satisfies the selection criteria. Although pulse pileup in high photon flux conditions can result in an overestimation of the photons' energy, we can reasonably exclude this effect from being responsible for the large 43 MeV energy deposit. In fact, this count is due to two triggered adjacent scintillating bars, in both of which the reconstructed position of interaction, obtained according to the techniques illustrated in the work by *Labanti et al.* [2009], are compatible with each other. This configuration, together with the time coincidence of the two signals, suggests a localized interaction and is unlikely to be due to different independent photons. Analysis of the GRID data, which can potentially extend the maximum detected energy further, is in progress and the results will be reported in a forthcoming paper. A search for SuperAGILE counts in the corresponding MCAL time intervals was performed with negative results. This is not surprising because of the SuperAGILE energy range (18–60 keV), its very small effective area for higher-energy photons and its limited field of view.

5. Comparison With the First RHESSI TGF Catalog

[24] In this section we compare the MCAL results with those reported in the first RHESSI TGF catalog [*Grefenstette et al.*, 2009]. The RHESSI detectors' effective area for isotropic photons is ~250 cm^2 at 1 MeV; a description of the RHESSI spectrometer is reported in the work by *Smith et al.* [2002]. For this comparison we considered the RHESSI TGFs detected at latitudes lower than 2.5 degrees in absolute value, to be compliant with the AGILE orbit. RHESSI data were retrieved from the publicly available online repository at http://scipp. ucsc.edu/dsmith/tgflib_public/.

Table 3. Average Properties of the Selected Events in Tables 1 and 2

Physical Property	Average Value
Duration	(1.5 ± 0.8) ms
Number of counts	17 ± 5
Peak flux in 200 μs	6 ± 2
Photon energy	(3.9 ± 1.4) MeV
Hardness ratio	1.5 ± 0.7
Maximum photon energy	(16 ± 8) MeV
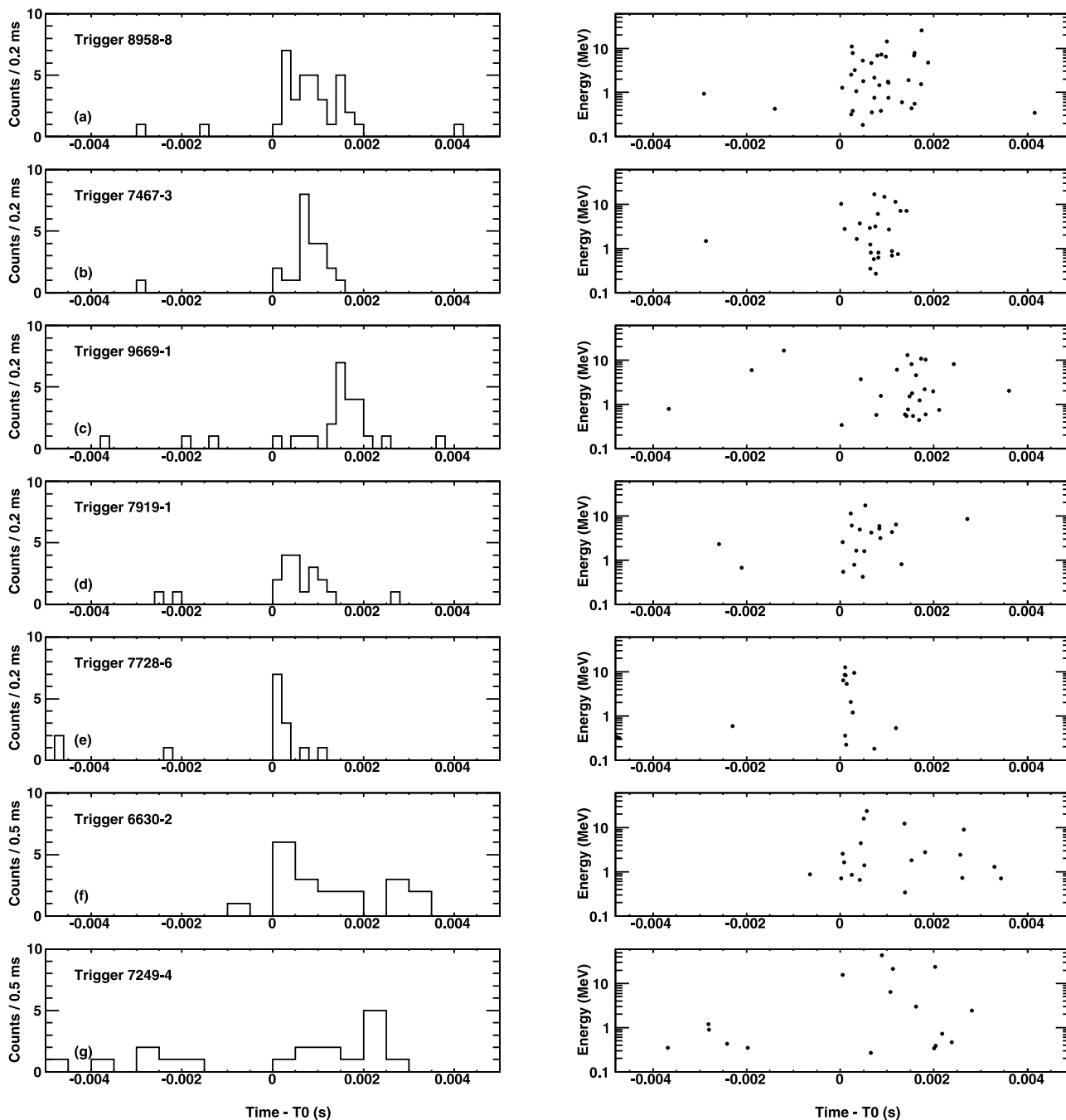
Figure 3. (left) Light curves and (right) energy versus time plots for several TGF candidates. (a–c) The three brightest events. (d) The event with the largest hardness ratio. (e) The shortest event. (f) The longest-duration event. (g) The event with the highest-energy photon.

5.1. Geographical and Local Time Trigger Distributions

[25] In addition to the latitude selection reported above, for the comparison of the geographical and local time distributions, the RHESSI TGF sample considered consists of 61 TGFs recorded in the months from June to March, consistent with the AGILE observation period. Moreover, only events before 1 January 2006 were considered, as recommended by *Grefenstette et al.* [2009], in order to exclude the 2006–2007 period for which the instrument response is still under study due to radiation damage of the RHESSI detectors.

[26] Figure 6 shows the comparison between the RHESSI and MCAL distributions for longitude and local time. Each distribution was normalized to the total number of counts in the sample. A good agreement between the two distributions is evident, indicating that the overall selection criteria we adopted are selecting a sample of events compatible with that of RHESSI.
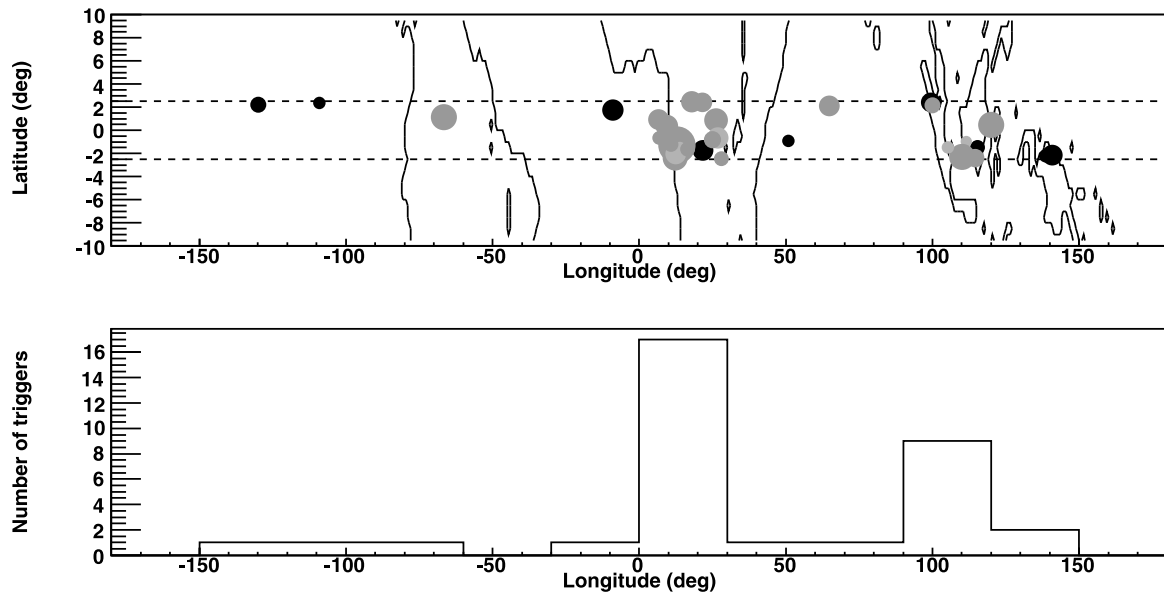
Figure 4. Geographical distribution of the selected triggers. (top) Scatterplot of the geographical foot-print of the AGILE satellite for the selected events. The radius of each dot is proportional to the number of counts; the color indicates the hardness ratio (the brightest being the hardest) according to the data reported in Table 2. The dashed horizontal lines mark the maximum latitudes reached by AGILE. (bottom) Longitude distribution of the sample.
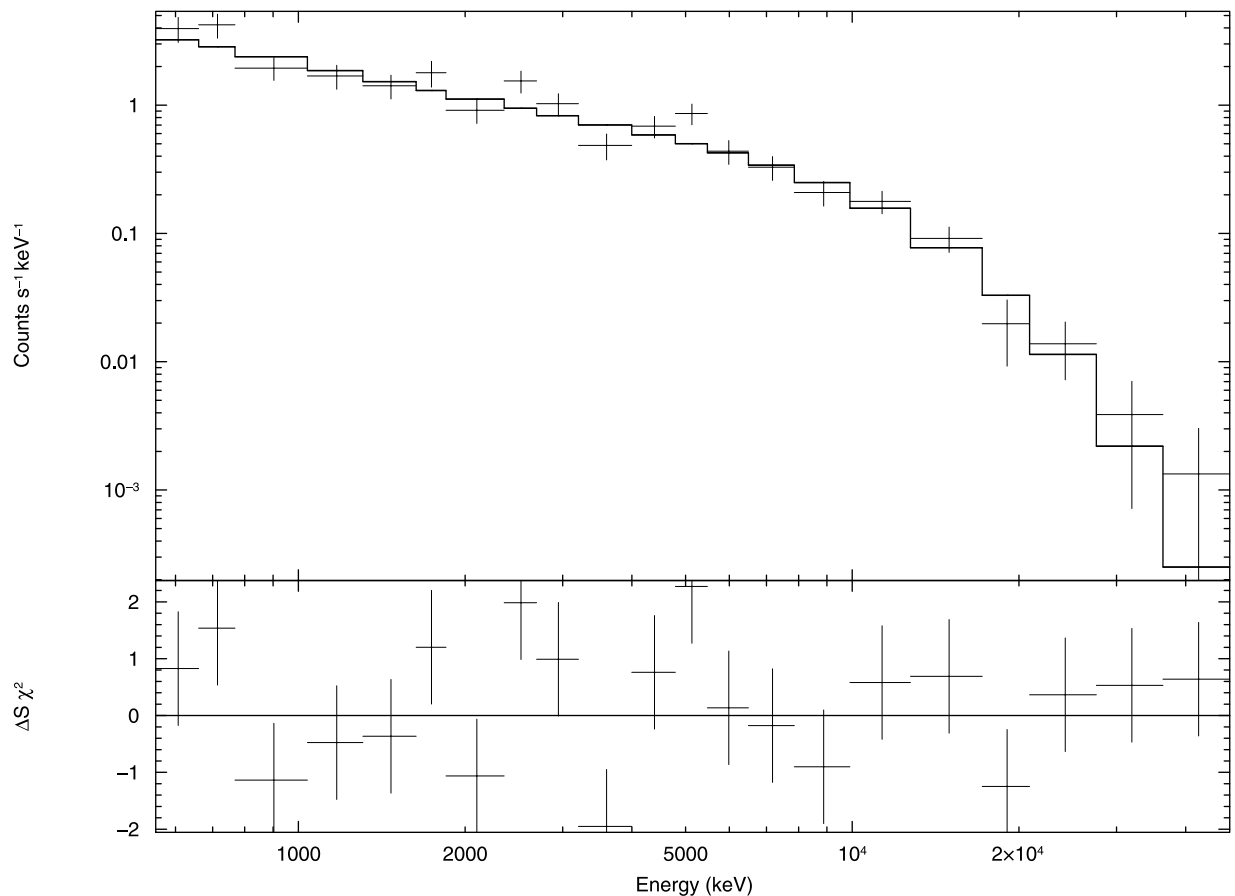
Figure 5. (top) Cumulative background-subtracted count spectrum for the MCAL TGF sample. A cutoff power law best fit model convolved with the instrumental response (see text for details) is superimposed on the data (solid line). (bottom) The residual distribution.
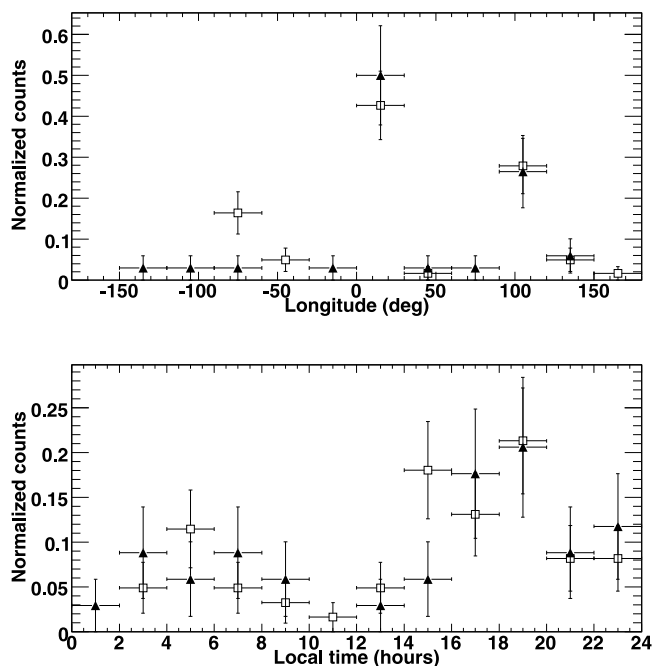
Figure 6. (top) Geographic longitude and (bottom) local time distributions for AGILE (solid triangles) and RHESSI (open squares) TGFs samples. The vertical axis error bars are one standard deviation assuming Poisson distribution.

5.2. Cumulative Spectra

[27] For the spectral comparison, the RHESSI TGF sample considered consists of 62 TGFs detected at latitudes lower than 2.5 degrees in absolute value before 1 January 2005, as recommended by *Grefenstette et al.* [2009] for spectroscopic analysis. Concerning the MCAL spectrum reported in section 4.2, it must be noted that the counts have been cumulated in the time interval corresponding to the TGF duration, as obtained from visual inspection of the light curves of the candidates. This has been done in order to maximize the signal-to-noise ratio and is only possible because of the limited background. However, for the RHESSI spectrum all the counts provided for a 10 ms time interval including the TGF have been cumulated. In order to directly compare the unfolded AGILE-MCAL model to the RHESSI data, a new MCAL spectrum was produced cumulating the counts in a 10 ms time interval surrounding the TGF as well. This spectrum was fitted with a cutoff power law model in the energy range 500 keV to 40 MeV, resulting in a spectral index $\alpha = 0.45^{+0.26}_{-0.33}$ and a high-energy cutoff energy $\beta = 8.8^{+3.5}_{-2.4}$ MeV, with a reduced χ^2 of 1.3 with 18 degrees of freedom. All quoted errors are at the 90% confidence level. This model is compatible with that obtained previously apart from the normalization constant, as expected because of the different integration time. The best fit AGILE-MCAL model was then convolved with the RHESSI detector response matrix, provided by the RHESSI team together with the TGF
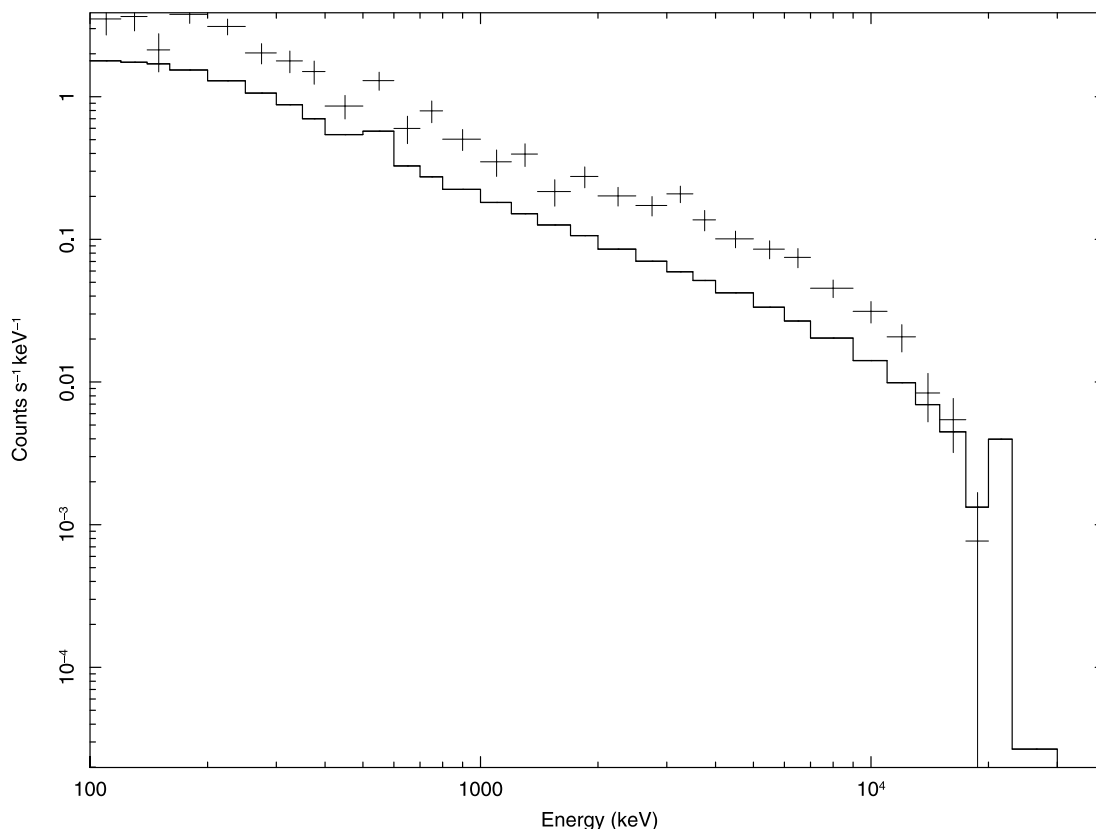
Figure 7. RHESSI experimental cumulative count spectrum for events triggered before 1 January 2005 at latitudes lower than 2.5° in absolute value. The solid curve is the MCAL best fit model convolved with the RHESSI response matrix.
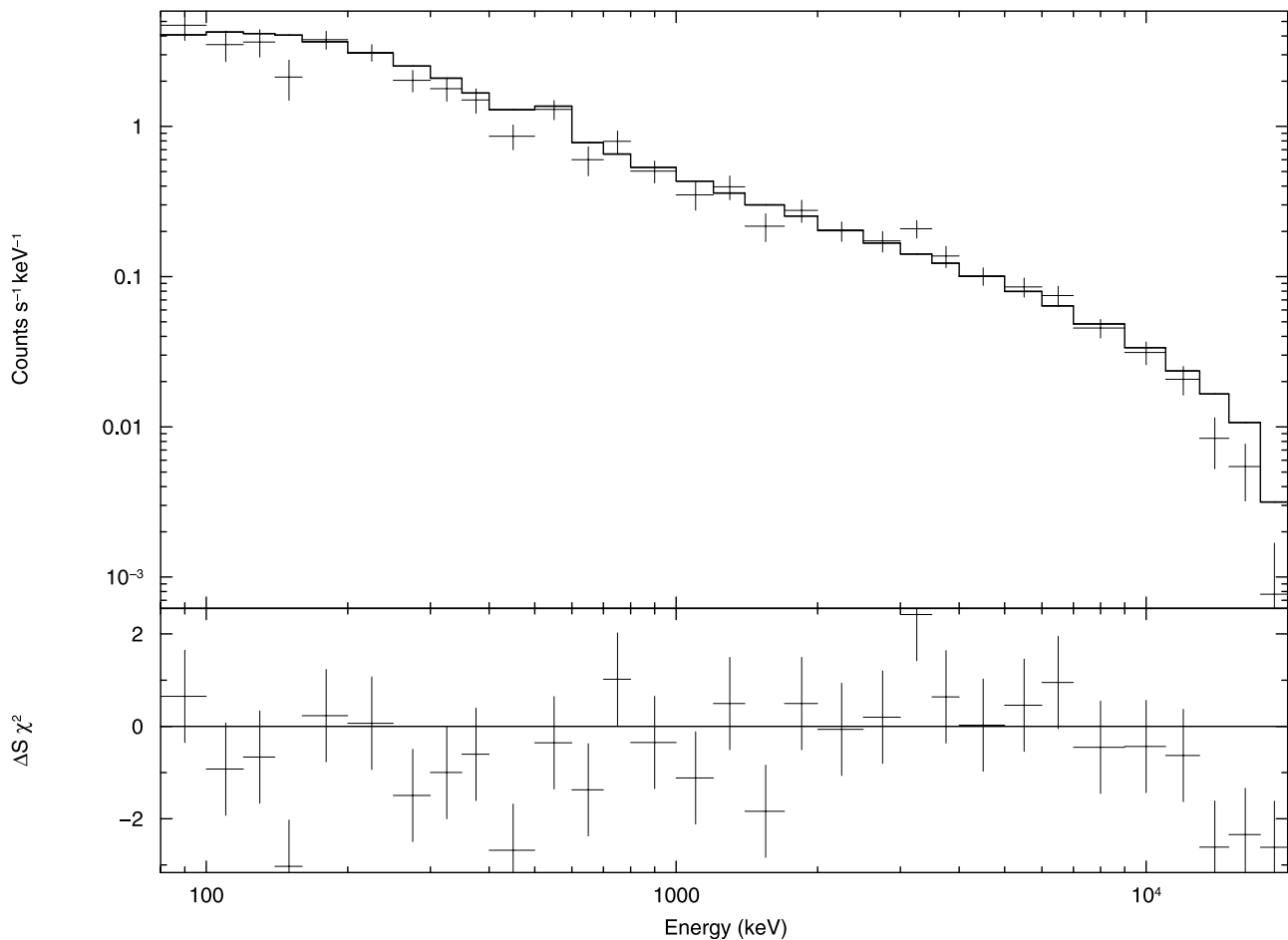
Figure 8. RHESSI experimental cumulative count spectrum for events triggered before 1 January 2005 at latitudes lower than 2.5° in absolute value. (top) The solid curve is the MCAL best fit model convolved with the RHESSI response matrix after the normalization factor is fit to RHESSI data (spectral parameters are kept constant). (bottom) The fit residuals.

catalog, to obtain the expected RHESSI count spectrum. Figure 7 shows the RHESSI count spectrum for the selected TGF sample (data points) and the expected RHESSI count spectrum for the AGILE-MCAL best fit model reported above (solid curve).

[28] First of all, a good agreement between the two instruments concerning the overall spectral shape can be noted. Below 500 keV the spectral differences should not be considered since the MCAL model spectrum is valid only above that energy. If the spectral parameters of the model are frozen and only the normalization constant is allowed to vary, a good fit in the energy range 500 keV to 10 MeV is obtained, with a reduced χ^2 of 1.06 with 15 degrees of freedom, and a normalization constant a factor of 2.3 that obtained previously for MCAL. The fit results are shown in Figure 8. According to these results it seems that MCAL selects a TGF population fainter than that of RHESSI. Possible reasons for this include differences in absolute flux calibration, differences in trigger criteria, and different effects of dead time.

[29] Of course we cannot exclude a slight difference in absolute flux calibration. Cross calibration, for example on cosmic gamma ray bursts detected by both instruments, could

be useful to clarify this issue. Moreover, the use of a fixed-angle response matrix could be responsible for a shift in the normalization constant, as discussed in section 4.2.

[30] The detection of a fainter-than-RHESSI population could also be due to the lower background exhibited by MCAL with respect to RHESSI. In this case, a much larger sample should be detected, which is not the case. This could be due to excessively conservative selection criteria.

[31] A critical issue possibly affecting MCAL results is dead time. It has been demonstrated that RHESSI TGFs are heavily affected by dead time; the RHESSI detectors were almost always counting at the maximum allowed rate during the brightest part of the TGF [*Grefenstette et al.*, 2009]. This means that the intensity distribution of the RHESSI TGF is compressed toward lower values; therefore, it is not possible to determine the true TGF brightness distribution, i.e., the total amount of energy involved in the process. Since the TGF population detected by MCAL seems to be fainter than that of RHESSI, dead time may also affect the MCAL results. Further investigations in this direction should be driven by Monte Carlo simulations. In any case, the overall consistency between the RHESSI and MCAL spectral

parameters confirms the validity of the selection criteria applied to the MCAL events.

6. Summary and Conclusions

[32] The MCAL instrument on board the AGILE satellite detects a population of millisecond time scale, very hard bursts of gamma rays with average characteristics compatible with those of TGFs. With the current trigger configuration and selection criteria a sample of 34 events have been identified, with an average detection rate of ~4 events/month. Since the full activation of the trigger logic on the 1 ms time scale in March 2009, the detection rate has almost doubled. The geographical and local time distributions of the events is consistent with that of the RHESSI TGFs when an event sample corresponding to the AGILE orbit is considered. The cumulative spectra of the AGILE and RHESSI samples can be fit by the same functional form in the 500 keV to 10 MeV energy range, apart from a small factor in the normalization constant. In our opinion, the remarkable consistency between the properties of the AGILE and RHESSI samples strongly confirms that the AGILE population is due to TGFs as well.

[33] The difference in the intensity distribution between AGILE and RHESSI could be due to calibration issues, the trigger selection criteria, and/or the contribution of dead time. To disentangle these contributions, dedicated analysis will be performed. A critical review of the selection criteria could reveal a larger TGF population rejected by the current algorithms.

[34] Our data show that impulsive TGF particle acceleration produces electron kinetic energies well above a few tens of MeV. Several photons with energies above 20 MeV are detected, the maximum being 43 MeV. Our data then determine an important constraint for the theoretical modeling of particle acceleration and atmospheric transport during and following TGF events. Furthermore, AGILE-MCAL spectral data show with high confidence that the spectrum is an effective Bremsstrahlung with a typical exponential cutoff of photon energy near 10 MeV. The obtained cutoff energy is consistent with the average energy of 7.2 MeV expected for an electron population undergoing RREA, as reported in the work by *Dwyer* [2004] and *Dwyer and Smith* [2005].

[35] An important scientific contribution to TGF science may come from the excellent AGILE absolute time resolution, experimentally confirmed to be better than 200 μs and continuing to improve with increased statistics. Such a high time resolution could allow correlation with precise lightning geolocation by means of sferics observation, producing significant constraints on emission models by precisely assessing the time delay between TGFs and the associated lightning stroke. For this reason, a high priority should be placed on the correlation of the AGILE events with sferics.

References

Argan, A., et al. (2004), The data handling system for the AGILE satellite, in *Conference Record of the IEEE Nuclear Science Symposium, October 16–22, 2004, Rome, Italy*, pp. 371–375, Inst. of Electr. and Electron. Eng., New York.

Cohen, M. B., U. S. Inan, and G. Fishman (2006), Terrestrial gamma ray flashes observed aboard the Compton Gamma Ray Observatory/Burst and Transient Source Experiment and ELF/VLF radio atmospherics, *J. Geophys. Res.*, *111*, D24109, doi:10.1029/2005JD006987.

Cummer, S. A., Y. Zhai, W. Hu, D. M. Smith, L. I. Lopez, and M. A. Stanley (2005), Measurements and implications of the relationship between lightning and terrestrial gamma ray flashes, *Geophys. Res. Lett.*, *32*, L08811, doi:10.1029/2005GL022778.

Dwyer, J. R. (2004), Implications of x-ray emission from lightning, *Geophys. Res. Lett.*, *31*, L12102, doi:10.1029/2004GL019795.

Dwyer, J. R. (2008), Source mechanisms of terrestrial gamma-ray flashes, *J. Geophys. Res.*, *113*, D10103, doi:10.1029/2007JD009248.

Dwyer, J. R., and D. M. Smith (2005), A comparison between Monte Carlo simulations of runaway breakdown and terrestrial gamma-ray flash observations, *Geophys. Res. Lett.*, *32*, L22804, doi:10.1029/2005GL023848.

Feroci, M., et al. (2007), SuperAGILE: The hard X-ray imager for the AGILE space mission, *Nucl. Instrum. Methods Phys. Res., Sect. A*, *581*, 728–754, doi:10.1016/j.nima.2007.07.147.

Fishman, G. J. (2009), TGF observations with the Gamma-ray Burst Monitor on the Fermi Observatory, paper presented at AGU Chapman Conference on Effects of Thunderstorms and Lightning in the Upper Atmosphere, AGU, State College, Pa., 10–14 May.

Fishman, G. J., and D. M. Smith (2008), Observations of two terrestrial gamma-ray flashes (TGFs) over a wide energy range with the Fermi Gamma-ray Burst Monitor, *Eos Trans. AGU*, *89*(53), Fall Meet. Suppl., Abstract AE21A-02.

Fishman, G. J., et al. (1989), BATSE: The Burst and Transient Source Experiment on the Gamma Ray Observatory, in *Proceedings of the Gamma Ray Observatory Science Workshop: 10–12 April 1989, Goddard Space Flight Center, Greenbelt, MD*, edited by N. Johnson, vol. 2, pp. 39–50, Goddard Space Flight Cent., Greenbelt, Md.

Fishman, G. J., et al. (1994), Discovery of intense gamma-ray flashes of atmospheric origin, *Science*, *264*, 1313–1316.

Fuschino, F., et al. (2008), Search of GRB with AGILE Minicalorimeter, *Nucl. Instrum. Methods Phys. Res., Sect. A*, *588*, 17–21, doi:10.1016/j.nima.2008.01.004.

Fuschino, F., et al. (2009), AGILE view of TGFs, *AIP Conf. Proc.*, *1118*, 46–51, doi:10.1063/1.3137712.

Grefenstette, B. W., D. M. Smith, J. R. Dwyer, and G. J. Fishman (2008), Time evolution of terrestrial gamma ray flashes, *Geophys. Res. Lett.*, *35*, L06802, doi:10.1029/2007GL032922.

Grefenstette, B. W., D. M. Smith, B. J. Hazelton, and L. I. Lopez (2009), First RHESSI terrestrial gamma ray flash catalog, *J. Geophys. Res.*, *114*, A02314, doi:10.1029/2008JA013721.

Gurevich, A. V., G. M. Milikh, and R. Roussel-Dupre (1992), Runaway electron mechanism of air breakdown and preconditioning during a thunderstorm, *Phys. Lett. A*, *165*, 463–468, doi:10.1016/0375-9601(92)90348-P.

Hazelton, B. J., B. W. Grefenstette, D. M. Smith, J. R. Dwyer, X.-M. Shao, S. A. Cummer, T. Chronis, E. H. Lay, and R. H. Holzworth (2009), Spectral dependence of terrestrial gamma-ray flashes on source distance, *Geophys. Res. Lett.*, *36*, L01108, doi:10.1029/2008GL035906.

Inan, U. S., S. C. Reising, G. J. Fishman, and J. M. Horack (1996), On the association of terrestrial gamma-ray bursts with lightning and implications for sprites, *Geophys. Res. Lett.*, *23*, 1017–1020, doi:10.1029/96GL00746.

Labanti, C., et al. (2009), Design and construction of the MiniCalorimeter of the AGILE satellite, *Nucl. Instrum. Methods Phys. Res., Sect. A*, *598*, 470–479, doi:10.1016/j.nima.2008.09.021.

Longo, F., M. Marisaldi, F. Fuschino, C. Labanti, and M. Galli (2008), The AGILE-MCAL instrument as TGF monitor, *Eos Trans. AGU*, *89*(53), Fall Meet. Suppl., Abstract AE21A-03.

Marisaldi, M., et al. (2008a), Gamma-ray burst detection with the AGILE minicalorimeter, *Astron. Astrophys.*, *490*, 1151–1156, doi:10.1051/0004-6361:200810562.

Marisaldi, M., et al. (2008b), In-flight performance of the AGILE minicalorimeter and its gamma-ray burst detection capabilities, *Proc. SPIE Int. Soc. Opt. Eng.*, *7011*, 11, pp., doi:10.1117/12.789182.

Marisaldi, M., et al. (2009), Observations of TGFs with AGILE, paper presented at AGU Chapman Conference on Effects of Thunderstorms and Lightning in the Upper Atmosphere, AGU, State College, Pa., 10–14 May.

Nemiroff, R. J., J. T. Bonnell, and J. P. Norris (1997), Temporal and spectral characteristics of terrestrial gamma flashes, *J. Geophys. Res.*, *102*, 9659–9666, doi:10.1029/96JA03107.

Østgaard, N. (2009), Production altitude, initial distributions and time delays for TGFs when instrumental deadtime effects are treated properly, AGU Chapman Conference on Effects of Thunderstorms and Lightning in the Upper Atmosphere, AGU, State College, Pa., 10–14 May.

Østgaard, N., T. Gjesteland, J. Stadsnes, P. H. Connell, and B. Carlson (2008), Production altitude and time delays of the terrestrial gamma flashes: Revisiting the Burst and Transient Source Experiment spectra, *J. Geophys. Res.*, *113*, A02307, doi:10.1029/2007JA012618.

Pellizzoni, A., M. Pilia, A. Possenti, et al. (2009), Hegh-resolution timing observations of spin-powered pulsars with the AGILE gamma-ray telescope, *Astrophys. J.*, *691*, 1618–1633.

Perotti, F., M. Fiorini, S. Incorvaia, E. Mattaini, and E. Sant'Ambrogio (2006), The AGILE anticoincidence detector, *Nuclear Instrum. Methods Phys. Res., Sect. A*, *556*, 228–236, doi:10.1016/j.nima.2005.10.016.

Prest, M., G. Barbiellini, G. Bordignon, G. Fedel, F. Liello, F. Longo, C. Pontoni, and E. Vallazza (2003), The AGILE silicon tracker: An innovative/γ-ray instrument for space, *Nucl. Instrum. Methods Phys. Res., Sect. A*, *501*, 280–287, doi:10.1016/S0168-9002(02)02047-8.

Roussel-Dupré, R., and A. V. Gurevich (1996), On runaway breakdown and upward propagating discharges, *J. Geophys. Res.*, *101*, 2297–2312, doi:10.1029/95JA03278.

Smith, D. M., et al. (2002), The RHESSI spectrometer, *Sol. Phys.*, *210*, 33–60, doi:10.1023/A:1022400716414.

Smith, D. M., et al. (2005), Terrestrial gamma-ray flashes observed up to 20 MeV, *Science*, *307*, 1085–1088.

Tavani, M., et al. (2008), The AGILE space mission, *Nucl. Instrum. Methods Phys. Res., Sect. A*, *588*, 52–62, doi:10.1016/j.nima.2008.01.023.

Tavani, M., et al. (2009), The AGILE mission, *Astron. Astrophys.*, *502*, 995–1013, doi:10.1051/0004-6361/200810527.

L. A. Antonelli, S. Colafrancesco, S. Cutini, D. Gasparrini, P. Giommi, C. Pittori, B. Preger, P. Santolamazza, and F. Verrecchia, ASI Science Data Center, Via E. Fermi 45, I-00044 Frascati, Roma, Italy.

A. Argan and G. De Paris, INAF, Viale del Parco Mellini 84, Roma, Italy.

G. Barbiellini, F. Longo, and E. Moretti, Dipartimento di Fisica, Università di Trieste, Via A. Valerio 2, I-34127 Trieste, Italy.

F. Boffelli, P. W. Cattaneo, and A. Rappoldi, INFN, Via Bassi 6, I-27100 Pavia, Italy.

A. Bulgarelli, G. Di Cocco, F. Gianotti, F. Fuschino, C. Labanti, M. Marisaldi, and M. Trifoglio, IASF, INAF, Via Gobetti 101, I-40129 Bologna, Italy. (marisaldi@iasfbo.inaf.it)

V. Cocco, E. Costa, F. D'Ammando, E. Del Monte, G. Di Persio, I. Donnarumma, Y. Evangelista, M. Feroci, I. Lapshov, F. Lazzarotto, L. Pacciani, G. Piano, G. Pucella, A. Rubini, P. Soffitta, E. Striani, M. Tavani, A. Trois, and V. Vittorini, IASF, INAF, Via del Fosso del Cavaliere 100, I-00133 Roma, Italy.

P. Caraveo, A. Chen, M. Fiorini, A. Giuliani, S. Mereghetti, F. Perotti, and A. Zambra, IASF, INAF, Via E. Bassini 15, I-20133 Milano, Italy.

A. Ferrari and T. Froysland, CIFS, Viale Settimio Severo 63, I-10133 Torino, Italy.

M. Galli, ENEA, Via Martiri di Monte Sole 4, I-40129 Bologna, Italy.

P. Lipari and D. Zanello, INFN, Università degli Studi di Roma "La Sapienza," P.le Aldo Moro 2, I-00185 Roma, Italy.

A. Morselli, P. Picozza, and S. Sabatini, INFN, Università degli Studi di Roma "Tor Vergata," Via della Ricerca Scientifica 1, I-00133 Roma, Italy.

A. Pellizzoni, Osservatorio Astronomico di Cagliari, INAF, Loc. Poggio dei Pini, Strada 54, I-09012, Capoterra (CA), Italy.

M. Pilia and M. Prest, Dipartimento di Fisica, Università dell'Insubria, Via Valleggio 11, I-22100 Como, Italy.

M. Rapisarda, ENEA, Via Enrico Fermi 45, I-00044 Frascati, Roma, Italy.

L. Salotti, Agenzia Spaziale Italiana, Viale Liegi 26, I-00198 Roma, Italy.

E. Vallazza, INFN, Via A. Valerio 2, I-34127 Trieste, Italy.

S. Vercellone, IASF, INAF, Via Ugo La Malfa 153, I-90146 Palermo, Italy.